



Robust load frequency control of nonlinear power networks

Sebastian Trip, Michele Cucuzzella, Claudio De Persis, Antonella Ferrara & Jacquélien M. A. Scherpen

To cite this article: Sebastian Trip, Michele Cucuzzella, Claudio De Persis, Antonella Ferrara & Jacquélien M. A. Scherpen (2020) Robust load frequency control of nonlinear power networks, International Journal of Control, 93:2, 346-359, DOI: [10.1080/00207179.2018.1557338](https://doi.org/10.1080/00207179.2018.1557338)

To link to this article: <https://doi.org/10.1080/00207179.2018.1557338>



© 2018 The Author(s). Published by Informa UK Limited, trading as Taylor & Francis Group



Published online: 25 Dec 2018.



Submit your article to this journal [↗](#)



Article views: 1822



View related articles [↗](#)



View Crossmark data [↗](#)



Citing articles: 6 View citing articles [↗](#)

Robust load frequency control of nonlinear power networks*

Sebastian Trip^a, Michele Cucuzzella^a, Claudio De Persis^a, Antonella Ferrara^b and Jacquelin M. A. Scherpen^a

^aJan C. Willems Center for Systems and Control, ENTEG, Faculty of Science and Engineering, University of Groningen, Groningen, Netherlands;

^bDipartimento di Ingegneria Industriale e dell'Informazione, University of Pavia, Pavia, Italy

ABSTRACT

This paper proposes a decentralised second-order sliding mode (SOSM) control strategy for load frequency control (LFC) in power networks, regulating the frequency and maintaining the net inter-area power flows at their scheduled values. The considered power network is partitioned into control areas, where each area is modelled by an equivalent generator including second-order turbine-governor dynamics, and where the areas are nonlinearly coupled through the power flows. Asymptotic convergence to the desired state is established by constraining the state of the power network on a suitably designed sliding manifold. This manifold is designed relying on stability considerations made on the basis of an incremental energy (storage) function. Simulation results confirm the effectiveness of the proposed control approach.

ARTICLE HISTORY

Received 2 March 2018
Accepted 29 November 2018

KEYWORDS

Sliding mode control;
decentralised control;
stability of nonlinear
systems; power systems
stability

1. Introduction

To operate the power network successfully, the total generation should match the total load demand and associated system losses. It is however common that over time mismatches occur, resulting in a deviation of the system frequency from its nominal value and in power flows between the areas that differ from their scheduled exchanges. A weighted combination of the deviations in the frequency and in the tie-line power flows is generally called the 'Area Control Error' (ACE). Reducing this error is achieved by the so-called load frequency control (LFC) or automatic generation control (AGC), where an appropriate control scheme changes governor setpoints to compensate for local load changes and to maintain the scheduled tie-line power flows (Kundur, Balu, & Lauby, 1994).

Since the power network can be regarded as one of the most important infrastructures, improving LFC received a considerable amount of attention from various research communities (Ibraheem, Kumar, & Kothari, 2005; Pandey, Mohanty, & Kishor, 2013). Particularly, due to the increasing share of renewable energy sources, it is unsure if the existing implementations are still adequate (Apostolopoulou, Domínguez-García, & Sauer, 2016). To cope with the increasing uncertainties affecting a control area and to improve the controllers performance, advanced control techniques have been proposed to redesign the conventional control schemes, such as passivity-based control (Pogromsky, Fradkov, & Hill, 1996), model predictive control (Ersdal, Imsland, & Uhlen, 2016), adaptive control (Zribi, Al-Rashed, & Alrifai, 2005) and fuzzy control (Chang & Fu, 1997).



In this work, we propose a new control strategy based on the sliding mode (SM) control methodology, which is a well-known robust control approach, especially useful to control

systems subject to modelling uncertainties and external disturbances (Edwards & Spurgen, 1998; Utkin, 1992). Since the power network is typically subject to modelling uncertainties and external disturbances (Furtat & Fradkov, 2015), there are indeed various SM-based approaches to improve the conventional LFC schemes (Dong, 2016; Mi, Fu, Wang, & Wang, 2013; Trip, Cucuzzella, Persis, van der Schaft, & Ferrara, 2018), possibly together with fuzzy logic (Ha, 1998), genetic algorithms (Vrdoljak, Perić, & Petrović, 2010), disturbances observers (Mi et al., 2016) and linear matrix inequalities (LMI) based control techniques (Prasad, Purwar, & Kishor, 2015).

1.1 Main contributions

Although the use of SMs in LFC has received a considerable amount of attention, the solution proposed in this work and the associated stability analysis differ substantially from the aforementioned works. Particularly, we notice that a common assumption in the literature is that the coupling between the control areas is linear. Instead, we consider a more realistic nonlinear coupling between the control areas, induced by the nonlinear power flow equations, which poses new challenges in the design of the sliding manifold. To the best of our knowledge, we are not aware of existing controllers for nonlinear power networks (including second-order turbine-governor dynamics) that *provably* achieve frequency regulation while maintaining the scheduled tie-line power flows. We summarise the main contributions of this work as follows:

- (1) The considered nonlinear power network model is more general than commonly considered in the analytical studies of LFC schemes. In this paper, we adopt the model of

CONTACT Sebastian Trip  s.trip@rug.nl  Jan C. Willems Center for Systems and Control, ENTEG, Faculty of Science and Engineering, University of Groningen, Nijenborgh 4, 9747 AG Groningen, Netherlands

*Preliminary results appeared in Trip, Cucuzzella, Ferrara, and De Persis (2017).

a power network partitioned into control areas, having an arbitrarily complex and meshed topology. Besides including the nonlinear coupling between the areas, we model the generation side by an equivalent generator including second-order turbine-governor dynamics. Particularly, the appearance of nonlinear power flows in combination with the second-order turbine-governor dynamics is challenging as it requires the development of a new nonlinear storage function for the stability analysis (Trip & De Persis, 2018).

- (2) SM control typically generates discontinuous control inputs that could lead to an undesired chattering effect (Utkin, 2016; Ventura & Fridman, 2016) and/or damage the system actuator. In this work, we argue that the use of higher order SM schemes are beneficial to LFC, as they result in a continuous control input, avoiding to possibly damage the (mechanical) turbine governor. Particularly, we focus on the suboptimal second-order sliding mode (SSOSM) control algorithm proposed in Bartolini, Ferrara, and Usai (1998a), and explicitly design a decentralised controller. Moreover, the convergence to the sliding manifold is obtained neither measuring the power demand, nor using load observers.
- (3) When the power network is constrained to the designed sliding manifold, the convergence towards the desired state is established relying on a Barbashin–Krasovskii–LaSalle invariance principle, and a *new* incremental storage function, composed of a commonly used incremental energy function (Trip, Bürger, & De Persis, 2016) and additional cross-terms. Particularly, the design of a nonlinear sliding function is inspired by the proposed nonlinear incremental storage function. A case study shows the effectiveness of the proposed controller and demonstrates that, besides the immediate application to LFC, the combined use of sliding mode control and other nonlinear control techniques can provide new insights and control strategies.

1.2 Outline

The present paper is organised as follows: In Section 2, the network model is introduced. In Section 3, the considered LFC problem is formulated. The proposed controller is described in Section 4. The stability of the controlled power network is studied in Section 5. Simulation results are reported and discussed in Section 6, while some conclusions are finally gathered in Section 7.

1.3 Notation

Let $\mathbf{0}$ be the vector of all zeros of suitable dimension and let $\mathbf{1}_n$ be the vector containing all ones of length n . The i th element of vector x is denoted by x_i . A constant signal is denoted by x^* . A steady-state solution to system $\dot{x} = \zeta(x)$, is denoted by \bar{x} , i.e. $\mathbf{0} = \zeta(\bar{x})$. In case the argument of a function is clear from the context, we occasionally write $\zeta(x)$ as ζ . Let $A \in \mathbb{R}^{n \times n}$ be a matrix. In case A is a positive definite (positive semi-definite) matrix, we write $A > 0$ ($A \geq 0$). The sign function is defined as

follows (Shtessel, Edwards, Fridman, & Levant, 2014):

$$\text{sgn}(x) := \begin{cases} -1 & \text{if } x < 0, \\ 1 & \text{if } x > 0, \end{cases} \quad (1)$$

and $\text{sgn}(0) \in [-1, 1]$.

2. Nonlinear power network model

In this section, the dynamic model of a power network partitioned into control areas is presented. The dynamic behaviour of a single control area is described by an aggregated load and an equivalent thermal power plant with a non-reheat turbine, which is commonly represented by second-order turbine-governor dynamics. A block diagram of the considered system with two control areas is represented in Figure 1 (see also Table 1 for the description of the used symbols). Consequently, the dynamic equations of the i th area are the following:

$$\begin{aligned} \dot{\delta}_i &= \omega_i^b \\ T_{pi} \dot{\omega}_i^b &= -(\omega_i^b - \omega^*) + K_{pi} P_{ti} - K_{pi} P_{di} \\ &\quad - K_{pi} \sum_{j \in \mathcal{A}_i} \frac{V_i^* V_j^*}{X_{ij}} \sin(\delta_i - \delta_j), \end{aligned} \quad (2)$$

where \mathcal{A}_i is the set of control areas connected to the i th area by transmission lines. Note that we assume that the network is lossless, which is generally valid in high-voltage transmission networks where the line resistance is negligible. Moreover, P_{ti} in (2) is the power generated by the i th plant, and it can be expressed as the output of the following second-order dynamical system that describes the behaviour of both the governor and the turbine:

$$\begin{aligned} T_{gi} \dot{P}_{gi} &= -\frac{1}{R_i} (\omega_i^b - \omega^*) - P_{gi} + u_i \\ T_{ti} \dot{P}_{ti} &= -P_{ti} + P_{gi}. \end{aligned} \quad (3)$$

In this paper, we aim at the design of a continuous control input u_i to achieve frequency regulation and to maintain the power flows at their desired (scheduled) values. These control objectives will be made explicit in the next section. First, we suggest a compact notation for the overall power network that is useful for the upcoming discussions.

The considered power network consists of n interconnected control areas, of which the topology is represented by a connected and undirected graph $\mathcal{G} = (\mathcal{V}, \mathcal{E})$, where the nodes $\mathcal{V} = \{1, \dots, n\}$, represent the control areas and the edges $\mathcal{E} \subset \mathcal{V} \times \mathcal{V} = \{1, \dots, m\}$, represent the transmission lines connecting the areas. The topology can be described by its corresponding incidence matrix $\mathcal{B} \in \mathbb{R}^{n \times m}$. Then, by arbitrarily labelling the ends of edge k with a '+' and a '-', one has that

$$\mathcal{B}_{ik} = \begin{cases} +1 & \text{if } i \text{ is the positive end of } k \\ -1 & \text{if } i \text{ is the negative end of } k \\ 0 & \text{otherwise.} \end{cases}$$

The dynamics of the overall power network can now be compactly written for all areas $i \in \mathcal{V}$ as

$$\begin{aligned} \dot{\eta} &= \mathcal{B}^T \omega \\ T_p K_p^{-1} \dot{\omega} &= -K_p^{-1} \omega + P_t - P_d - \mathcal{B} \Gamma \sin(\eta) \end{aligned} \quad (4)$$

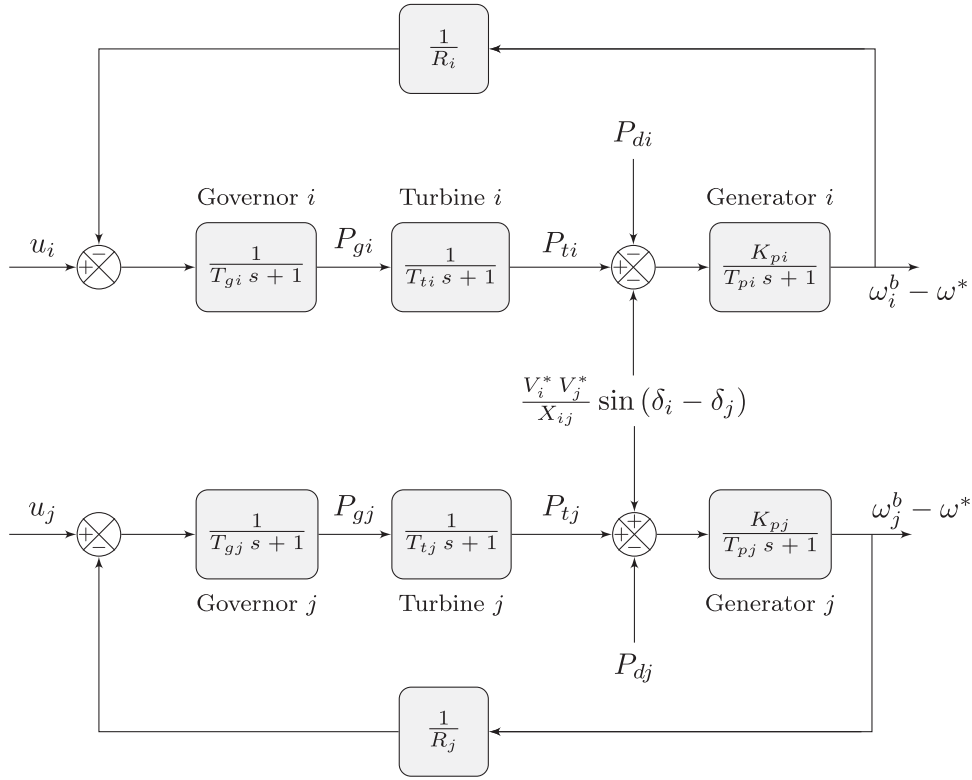


Figure 1. Block diagram of two interconnected control areas.

Table 1. Description of the used symbols.

Symbol	Description
δ_i	Voltage angle
ω_i^b	Frequency
ω_j	Frequency deviation
P_{ti}	Turbine output power
P_{gi}	Governor output
ω^*	Nominal frequency
T_{pi}	Time constant of the control area
T_{ti}	Time constant of the turbine
T_{gi}	Time constant of the governor
K_{pi}	Gain of the control area
R_i	Speed regulation coefficient
V_i^*	Constant voltage
X_{ij}	Line reactance
u_i	Control input
P_{di}	Unknown power demand

$$T_g \dot{P}_g = -R^{-1} \omega - P_g + u$$

$$T_t \dot{P}_t = -P_t + P_g,$$

where $\omega = \omega^b - \omega^* \mathbf{1}_n \in \mathbb{R}^n$ is the frequency deviation, $P_t \in \mathbb{R}^n$, $P_g \in \mathbb{R}^n$, $\Gamma = \text{diag}\{\Gamma_1, \dots, \Gamma_m\}$, with $\Gamma_k = V_i^* V_j^* / X_{ij}$, where line k connects areas i and j , $\sin(\eta) = (\sin(\eta_1), \dots, \sin(\eta_m))^T$, $P_d \in \mathbb{R}^n$ and $u \in \mathbb{R}^n$. Note furthermore that we introduced the variable $\eta = \mathcal{B}^T \delta \in \mathbb{R}^m$, where element η_k is the difference in voltage angles across line k between areas i and j . Matrices T_p, T_t, T_g, K_p, R are positive definite $n \times n$ diagonal matrices, e.g. $K_p = \text{diag}\{K_{p1}, \dots, K_{pn}\}$.

3. Problem formulation

Before focussing on the controller design, we formulate the two main objectives of LFC (automatic generation control). The first

objective is concerned with the steady-state frequency deviation $\bar{\omega}$, i.e. with $\lim_{t \rightarrow \infty} \omega(t)$.

Objective 1 (Frequency regulation):

$$\lim_{t \rightarrow \infty} \omega(t) = \bar{\omega} = \mathbf{0}. \quad (5)$$

Let $(\mathcal{B}P_f^*)_i$ denote the total desired power flow exchanged by control area $i \in \mathcal{V}$, P_f^* being an external reference signal. The second objective is to maintain the scheduled net power flows between the control areas.

Objective 2 (Maintaining scheduled net power flows):

$$\lim_{t \rightarrow \infty} \mathcal{B} \Gamma \sin(\eta(t)) = \mathcal{B} \Gamma \sin(\bar{\eta}) = \mathcal{B} P_f^*. \quad (6)$$

In case the power network does not contain cycles, Objective 2 is equivalent to $\lim_{t \rightarrow \infty} \Gamma \sin(\eta(t)) = P_f^*$, such that the power flow on every line is regulated towards its desired value (see also Remark 5.2 in Section 5). To be able to achieve Objectives 1 and 2, we make the following assumption on the feasibility of the control problem:

Assumption 3.1 (Feasibility): For a given constant P_d^* , there exist a constant input \bar{u} and state $(\bar{\omega} = \mathbf{0}, \bar{\eta}, \bar{P}_g, \bar{P}_t)$ that satisfies

$$\begin{aligned} \mathbf{0} &= \mathcal{B}^T \mathbf{0} \\ \mathbf{0} &= -K_p^{-1} \mathbf{0} + \bar{P}_t - P_d^* - \mathcal{B} \Gamma \sin(\bar{\eta}) \\ \mathbf{0} &= -R^{-1} \mathbf{0} - \bar{P}_g + \bar{u} \\ \mathbf{0} &= -\bar{P}_t + \bar{P}_g, \end{aligned} \quad (7)$$

where $\mathcal{B} \Gamma \sin(\bar{\eta}) = \mathcal{B} P_f^*$.

To increase the practical applicability, we furthermore desire the controllers to be decentralised and to be able to provide a continuous control input, avoiding to damage the turbine governor. We are now in a position to formulate the control problem:

Control Problem 1: Let Assumption 3.1 hold. Given system (4), design a decentralised control scheme, providing a continuous control input u , capable of guaranteeing that the controlled system is asymptotically stable with zero steady-state frequency deviation (Objective 1), maintaining, at the steady state, the scheduled (net) power flows (Objective 2).

4. The proposed robust solution

In this section, a decentralised SOSM control scheme is proposed to solve the aforementioned control problem. In this work, we focus on the well-established SSOSM controller proposed in Bartolini et al. (1998a) and apply it to the power network augmented with an additional state variable $\theta \in \mathbb{R}^n$ with dynamics

$$T_\theta \dot{\theta} = -\theta + P_t, \quad (8)$$

that will provide additional freedom to shape the transient behaviour. To facilitate the upcoming discussion, we recall for convenience the following definitions that are essential to sliding mode control:

Definition 4.1 (Sliding function): Consider system

$$\dot{x} = \zeta(x, u), \quad (9)$$

with state $x \in \mathbb{R}^n$, and input $u \in \mathbb{R}^m$. The *sliding function* $\sigma(x) : \mathbb{R}^n \rightarrow \mathbb{R}^m$ is a sufficiently smooth output function of system (9).

Definition 4.2 (r -sliding manifold): The r -sliding manifold¹ is given by

$$\{x \in \mathbb{R}^n, u \in \mathbb{R}^m : \sigma = L_\zeta \sigma = \dots = L_\zeta^{(r-1)} \sigma = \mathbf{0}\}, \quad (10)$$

where $L_\zeta^{(r-1)} \sigma(x)$ is the $(r-1)$ th order Lie derivative of $\sigma(x)$ along the vector field $\zeta(x, u)$. With a slight abuse of notation we also write $L_\zeta \sigma(x) = \dot{\sigma}(x)$, and $L_\zeta^{(2)} \sigma(x) = \ddot{\sigma}(x)$.

Definition 4.3 (r -order sliding mode (controller)): An r -order sliding mode is enforced from $t = T_r \geq 0$, when, starting from an initial condition, the state of (9) reaches the r -sliding manifold, and remains there for all $t \geq T_r$. The order of a *sliding mode controller* that enforces an r -order sliding mode is equal to r .

Bearing in mind the definitions above, we propose for the system at hand, the sliding function $\sigma(\omega, P_t, P_g, \theta, \eta) : \mathbb{R}^{4n+m} \rightarrow \mathbb{R}^n$ given by

$$\sigma = M_1 \omega + M_2 P_t + M_3 P_g + M_4 \theta + M_5 \mathcal{B}(\Gamma \sin(\eta) - P_f^*), \quad (11)$$

where M_1, \dots, M_5 are constant $n \times n$ diagonal matrices, suitable selected in order to assign the dynamics of the augmented

system on the manifold $\sigma = \mathbf{0}$. The sliding function (11) is stated in an ad-hoc manner to facilitate the discussion on the controller design. Nevertheless, the choice of (11) is inspired by the stability analysis in Section 5. Particularly, the permitted values for M_1, \dots, M_5 follow directly from the stability analysis, and we provide explicit values for these matrices in Assumption 5.1 in the next section.

Regarding the sliding function (11) as the output function² of system (4), (8), the relative degree³ is one. This implies that a first-order sliding mode controller can be *naturally* applied in order to make the state of the controlled system reach, in a finite time, the manifold $\sigma = \mathbf{0}$. However, a sliding mode controller typically generates a fast switching discontinuous control input that could lead to an undesired chattering effect (Utkin, 2016; Ventura & Fridman, 2016) and/or damage the actuator. As a consequence, it is important to provide a continuous control input u to the governor. To obtain a continuous input u , we adopt the procedure suggested in Bartolini et al. (1998a), yielding for system (4) augmented with (8):

$$\begin{aligned} \dot{\eta} &= \mathcal{B}^T \omega \\ T_p K_p^{-1} \dot{\omega} &= -K_p^{-1} \omega + P_t - P_d - \mathcal{B} \Gamma \sin(\eta) \\ T_g \dot{P}_g &= -R^{-1} \omega - P_g + u \\ T_t \dot{P}_t &= -P_t + P_g \\ T_\theta \dot{\theta} &= -\theta + P_t \\ \dot{u} &= w, \end{aligned} \quad (12)$$

where w is the new (discontinuous) input generated by a sliding mode controller discussed below. Note that indeed the input signal to the governor, $u(t) = \int_0^t w(\tau) d\tau$, is continuous, since, as will we show later, the input w is piecewise constant. Furthermore, a consequence of the previous procedure is that the system relative degree (with respect to the new control input w) is now two, and we need to rely on a second-order sliding mode control strategy to attain the sliding manifold $\sigma = \dot{\sigma} = \mathbf{0}$ in a finite time (Levant, 2003). To make the controller design explicit, we introduce two auxiliary variables $\xi_1 = \sigma$ and $\xi_2 = \dot{\sigma}$ and define the so-called auxiliary system as follows:

$$\begin{aligned} \dot{\xi}_1 &= \xi_2 \\ \dot{\xi}_2 &= \phi + Gw \\ \dot{u} &= w, \end{aligned} \quad (13)$$

where ξ_2 is not measurable as it depends, e.g. on the unknown power demand P_d . Bearing in mind (11) and that $\ddot{\sigma} = \phi + Gw$, it follows that $\phi \in \mathbb{R}^n$ and $G \in \mathbb{R}^{n \times n}$ are given by

$$\begin{aligned} \phi &= \left(M_1 T_p^{-2} + M_3 R^{-1} T_p^{-1} T_g^{-1} - M_2 R^{-1} T_t^{-1} T_g^{-1} \right. \\ &\quad \left. + M_3 R^{-1} T_g^{-2} \right) \omega - \left(M_1 K_p T_p^{-2} + M_3 K_p R^{-1} T_p^{-1} T_g^{-1} \right. \\ &\quad \left. + M_1 K_p T_p^{-1} T_t^{-1} - M_2 T_t^{-2} + M_4 T_t^{-1} T_\theta^{-1} + M_4 T_\theta^{-2} \right) P_t \\ &\quad + \left(M_1 K_p T_p^{-1} T_t^{-1} - M_2 T_t^{-2} - M_2 T_t^{-1} T_g^{-1} + M_3 T_g^{-2} \right. \\ &\quad \left. + M_4 T_t^{-1} T_\theta^{-1} \right) P_g + \left(M_2 T_t^{-1} - M_3 T_g^{-1} \right) T_g^{-1} u \end{aligned}$$

$$\begin{aligned}
& + \left(M_1 T_p^{-1} + M_3 R^{-1} T_g^{-1} \right) \left(K_p T_p^{-1} P_d + K_p T_p^{-1} \mathcal{B} \Gamma \sin(\eta) \right) \\
& - M_1 K_p T_p^{-1} \left(\dot{P}_d + \mathcal{B} \Gamma \frac{d}{dt} \sin(\eta) \right) \\
& + M_5 \mathcal{B} \Gamma \frac{d^2}{dt^2} \sin(\eta) + M_4 T_\theta^{-2} \theta, \\
G & = M_3 T_g^{-1}. \tag{14}
\end{aligned}$$

Note that, ϕ , G are uncertain due to the presence of the unmeasurable power demand P_d and possible parameter uncertainties. However, we assume that ϕ and G can be bounded.

Assumption 4.1 (Bounded uncertainty): *The terms ϕ_i and G_{ii} in (13) have known bounds, i.e.*

$$\|\phi_i\| \leq \Phi_i \quad \forall i \in \mathcal{V} \tag{15}$$

$$0 < G_i^{\min} \leq G_{ii} \leq G_i^{\max} \quad \forall i \in \mathcal{V}, \tag{16}$$

Φ_i , G_i^{\min} and G_i^{\max} being positive constants.

To steer ξ_{1i} and ξ_{2i} to zero in a finite time even in the presence of the uncertainties, the SSOSM algorithm (Bartolini et al., 1998a) is used. Consequently, the control law for the i th node is given by

$$w_i = -\alpha_i W_i \operatorname{sgn} \left(\xi_{1i} - \frac{1}{2} \xi_{1i}^{\max} \right), \tag{17}$$

with

$$W_i > \max \left(\frac{\Phi_i}{\alpha_i^* G_i^{\min}}; \frac{4\Phi_i}{3G_i^{\min} - \alpha_i^* G_i^{\max}} \right), \tag{18}$$

$$\alpha_i^* \in (0, 1] \cap \left(0, \frac{3G_i^{\min}}{G_i^{\max}} \right), \tag{19}$$

α_i switching between α_i^* and 1, according to Bartolini et al. (1998a, Algorithm 1). The extremal values ξ_{1i}^{\max} in (17) can be detected by implementing for instance a peak detection as in Bartolini, Ferrara, and Usai (1998b)⁴, or by checking $\operatorname{sgn}(\dot{\sigma})$, where $\dot{\sigma}$ can be estimated by implementing the well-known Levant differentiator (Levant, 2003).

Remark 4.1 (Adaptive SSOSM): In practical cases, the bounds in (15) and (16) can be determined relying on e.g. data analysis or physical insights. However, if these bounds cannot be estimated a priori, the adaptive version of the SSOSM algorithm proposed in Incremona, Cucuzzella, and Ferrara (2016) can be used to dominate the effect of the uncertainties.

Remark 4.2 (Local measurements): Because M_1, \dots, M_5 are diagonal matrices, each sliding variable σ_i is defined by only local variables at area $i \in \mathcal{V}$ and the overall control scheme is indeed decentralised.

Remark 4.3 (Second-order sliding modes): In order to constrain system (4) augmented with dynamics (8) on the sliding manifold $\sigma = \dot{\sigma} = \mathbf{0}$, any other SOSM control law can be used, such as the super-twisting control algorithm proposed in Levant (1993), which requires only the measurement of σ .

5. Stability analysis

In this section, we study the stability of the power network controlled by the proposed control scheme. To do so, we first show that the closed-loop system reaches in finite time the sliding manifold $\sigma = \dot{\sigma} = \mathbf{0}$. Second, to study the (nonlinear) system restricted to that manifold, we suggest an incremental storage function that under suitable conditions attains a local minimum at the desired steady state. Third, the desired convergence result is obtained by invoking the Barbashin–Krasovskii–LaSalle invariance principle.

In order to prove the stability, we require two (nonrestrictive) assumptions. First, we notice that the matrices M_1, \dots, M_5 , in (11) can be freely designed to obtain a suitable sliding manifold. As we will show, the upcoming stability analysis suggests the possible values for M_1, \dots, M_5 , leading to the following assumption:

Assumption 5.1 (Desired sliding manifold): *Let $M_1 > 0$, $M_2 \geq 0$, $M_3 > 0$ diagonal matrices and let M_4 and M_5 be defined as*

$$\begin{aligned}
M_4 & = -(M_2 + M_3) \\
M_5 & = M_1 X,
\end{aligned} \tag{20}$$

where X is a diagonal matrix satisfying⁵

$$0 < T_p K_p^{-1} - X T_p K_p^{-1} \mathcal{B} \Gamma [\cos(\bar{\eta})] \mathcal{B}^T K_p^{-1} T_p X, \tag{21}$$

and

$$\begin{aligned}
0 < K_p^{-1} - \frac{1}{4} K_p^{-1} X K_p^{-1} - \frac{1}{2} (T_p K_p^{-1} X \mathcal{B} \Gamma [\cos(\eta)] \mathcal{B}^T \\
+ \mathcal{B} \Gamma [\cos(\eta)] \mathcal{B}^T X K_p^{-1} T_p).
\end{aligned} \tag{22}$$

Remark 5.1 (Required information on the network topology): The value of X needs to be calculated once for the whole network and can be determined offline. The obtained value of X_{ii} needs then to be transmitted to control area i . Since all M_i are diagonal, the proposed control scheme is fully decentralised once the value of X is obtained. To facilitate the controller design that improves the scalability of the proposed solution, we provide a simple algorithm to determine a value of X satisfying (21) and (22) in Section 5.1

Second, the following assumption is made on the differences of voltage angles at steady state, which is generally satisfied under normal operating conditions of the power network.

Assumption 5.2 (Steady state voltage angles): *The differences in voltage angles in (7) satisfy*

$$\bar{\eta} \in \left(-\frac{\pi}{2}, \frac{\pi}{2} \right)^m. \tag{23}$$

The restrictions on M_i and $\bar{\eta}$ are required to apply the invariance principle later on in Theorem 5.1, where stability of the proposed control scheme is proven. This shows how the sliding manifold can be designed relying on an energy (storage) function-based stability analysis. Before discussing this main result, some useful intermediate results are derived. First, we

show that the SOSM controller (11)–(19) constrains the system in finite time to the manifold characterised in the lemma below.

Lemma 5.1 (Convergence to the sliding manifold): *Let Assumptions 3.1–5.1 hold. System (4) augmented with (8) converges in a finite time $T_r \geq 0$ to the manifold where*

$$P_g = -M_3^{-1}(M_1\omega + M_2P_t + M_4\theta + M_5\mathcal{B}(\Gamma \sin(\eta) - P_f^*)). \quad (24)$$

Proof: Following Bartolini et al. (1998a), the application of (17)–(19) to each control area guarantees that an SOSM is enforced, i.e. $\exists T_r \geq 0 : \sigma(t) = \dot{\sigma}(t) = \mathbf{0}, \forall t \geq T_r$, where T_r is the so-called reaching time. Then, from the definition of σ in (11), one can easily obtain (24), where M_3 is invertible since, according to Assumption 5.1, $M_3 > 0$. ■

Exploiting relation (24), the equivalent system on the sliding manifold is as follows:

$$\begin{aligned} \dot{\eta} &= \mathcal{B}^T \omega \\ T_p K_p^{-1} \dot{\omega} &= -K_p^{-1} \omega + P_t - P_d - \mathcal{B} \Gamma \sin(\eta) \\ M_1^{-1} M_3 T_t \dot{P}_t &= -M_1^{-1} (M_2 + M_3) P_t - M_1^{-1} M_4 \theta \\ &\quad - \omega - M_1^{-1} M_5 \mathcal{B} (\Gamma \sin(\eta) - P_f^*) \\ T_\theta \dot{\theta} &= -\theta + P_t \\ \sigma &= \mathbf{0}, \end{aligned} \quad (25)$$

where we include the additional dynamic (8). As we now focus on the asymptotic convergence of the equivalent system to a desired steady state satisfying Objective 1 and Objective 2, we make the following assumption (see also Remark 5.3), which is required in order to allow for a steady state solution.

Assumption 5.3 (Constant power demand): *The power demand (unmatched disturbance) P_d^* is constant.*

As a consequence of Assumptions 3.1 and 5.3, there exists a $(\bar{\omega} = \mathbf{0}, \bar{\eta}, \bar{P}_t, \bar{\theta})$ satisfying

$$\begin{aligned} \mathbf{0} &= \mathcal{B}^T \mathbf{0} \\ \mathbf{0} &= -K_p^{-1} \mathbf{0} + \bar{P}_t - P_d^* - \mathcal{B} \Gamma \sin(\bar{\eta}) \\ \mathbf{0} &= -M_1^{-1} (M_2 + M_3) \bar{P}_t - M_1^{-1} M_4 \bar{\theta} - \mathbf{0} \\ &\quad - M_1^{-1} M_5 \mathcal{B} (\Gamma \sin(\bar{\eta}) - P_f^*) \\ \mathbf{0} &= -\bar{\theta} + \bar{P}_t \\ \sigma &= \mathbf{0}, \end{aligned} \quad (26)$$

where in (7), $\bar{P}_g = \bar{\theta} = \bar{u}$. To show the desired convergence properties of the equivalent system (25) we consider the function

$$\begin{aligned} S(\omega, \eta, P_t, \theta) &= \frac{1}{2} \omega^T T_p K_p^{-1} \omega - \mathbf{1}^T \Gamma \cos(\eta) \\ &\quad + \omega^T T_p K_p^{-1} X \mathcal{B} \Gamma \sin(\eta) + \frac{1}{2} P_t^T M_1^{-1} M_3 T_t P_t \\ &\quad + \frac{1}{2} \theta^T M_1^{-1} (M_2 + M_3) T_\theta \theta, \end{aligned} \quad (27)$$

that consists of an energy function of the power network (Trip et al., 2016), a cross-term and common quadratic functions for

the states of the turbine and the auxiliary dynamics. The stability of the system is then proven using an incremental storage function that is the Bregman distance (Bregman, 1967) associated to the function (27). The Bregman distance associated to S is defined as:

$$\begin{aligned} S_B &= S(\omega, \eta, P_t, \theta) - S(\mathbf{0}, \bar{\eta}, \bar{P}_t, \bar{\theta}) \\ &\quad - \frac{\partial S}{\partial \omega} \Big|_{x=\bar{x}}^T (\omega - \mathbf{0}) - \frac{\partial S}{\partial \eta} \Big|_{x=\bar{x}}^T (\eta - \bar{\eta}) - \frac{\partial S}{\partial P_t} \Big|_{x=\bar{x}}^T (P_t - \bar{P}_t) \\ &\quad - \frac{\partial S}{\partial \theta} \Big|_{x=\bar{x}}^T (\theta - \bar{\theta}) \\ &= \frac{1}{2} \omega^T T_p K_p^{-1} \omega - \mathbf{1}^T \Gamma \cos(\eta) + \mathbf{1}^T \Gamma \cos(\bar{\eta}) \\ &\quad - (\Gamma \sin(\bar{\eta}))^T (\eta - \bar{\eta}) + \omega^T T_p K_p^{-1} X \mathcal{B} (\Gamma \sin(\eta) - \Gamma \sin(\bar{\eta})) \\ &\quad + \frac{1}{2} (P_t - \bar{P}_t)^T M_1^{-1} M_3 T_t (P_t - \bar{P}_t) \\ &\quad + \frac{1}{2} (\theta - \bar{\theta})^T M_1^{-1} (M_2 + M_3) T_\theta (\theta - \bar{\theta}), \end{aligned} \quad (28)$$

where $x = (\omega, \eta, P_t, \theta)$ and $\bar{x} = (\mathbf{0}, \bar{\eta}, \bar{P}_t, \bar{\theta})$ satisfies (26). We remark that the Bregman distance S_B is equal to S minus the first-order Taylor expansion of S around $(\mathbf{0}, \bar{\eta}, \bar{P}_t, \bar{\theta})$. We now derive two useful properties of S_B , namely that S_B has a local minimum at $(\mathbf{0}, \bar{\eta}, \bar{P}_t, \bar{\theta})$ and that $\dot{S}_B \leq 0$. We start with the first claim.

Lemma 5.2 (Local minimum of S_B): *Let Assumptions 3.1–5.3 hold. Then S_B has a local minimum at $(\mathbf{0}, \bar{\eta}, \bar{P}_t, \bar{\theta})$.*

Proof: Since S_B is a Bregman distance associated to (27), it is sufficient to show that (27) is convex at the point $(\mathbf{0}, \bar{\eta}, \bar{P}_t, \bar{\theta})$ in order to infer that S_B has a local minimum at that point. We consider therefore the Hessian matrix $H(S(\omega, \eta, P_t, \theta))$, evaluated at $(\mathbf{0}, \bar{\eta}, \bar{P}_t, \bar{\theta})$, which we briefly denote $\bar{H}(S)$. A straightforward calculation shows that

$$\bar{H}(S) = \begin{bmatrix} Q & \mathbf{0} \\ \mathbf{0} & M \end{bmatrix}, \quad (29)$$

with

$$Q = \begin{bmatrix} T_p K_p^{-1} & T_p K_p^{-1} X \mathcal{B} \Gamma [\cos(\bar{\eta})] \\ [\cos(\bar{\eta})] \Gamma \mathcal{B}^T X K_p^{-1} T_p & \Gamma [\cos(\bar{\eta})] \end{bmatrix} \quad (30)$$

$$M = \begin{bmatrix} M_1^{-1} M_3 T_t & \mathbf{0} \\ \mathbf{0} & M_1^{-1} (M_2 + M_3) T_\theta \end{bmatrix}. \quad (31)$$

It is immediate to see that $M > 0$, such that $\bar{H}(S) > 0$ if and only if $Q > 0$. Since $\Gamma [\cos(\bar{\eta})] > 0$ as a result of Assumption 5.2, it is sufficient that the Schur complement of block $\Gamma [\cos(\bar{\eta})]$ of matrix Q satisfies

$$0 < T_p K_p^{-1} - X T_p K_p^{-1} \mathcal{B} \Gamma [\cos(\bar{\eta})] \mathcal{B}^T K_p^{-1} T_p X. \quad (32)$$

The claim then follows from Assumption 5.1. ■

We now show that S_B satisfies $\dot{S}_B \leq 0$ along the solutions to (25).

Lemma 5.3 (Evolution of S_B): *Let Assumptions 3.1–5.3 hold. Then $\dot{S}_B \leq 0$.*

Proof: We have that

$$\begin{aligned} \dot{S}_B &= \omega^T (-K_p^{-1} \omega + P_t - P_d^* - \mathcal{B}\Gamma \sin(\eta)) + (\Gamma \sin(\eta)) \\ &\quad - \Gamma \sin(\bar{\eta}))^T \mathcal{B}^T \omega + \omega^T T_p K_p^{-1} X \mathcal{B}\Gamma [\cos(\eta)] \mathcal{B}^T \omega \\ &\quad + (\mathcal{B}\Gamma (\sin(\eta) - \sin(\bar{\eta})))^T X (-K_p^{-1} \omega + P_t - P_d^* \\ &\quad - \mathcal{B}\Gamma \sin(\eta)) + (P_t - \bar{P}_t)^T (-M_1^{-1} (M_2 + M_3) P_t \\ &\quad - M_1^{-1} M_4 \theta - \omega - M_1^{-1} M_5 \mathcal{B} (\Gamma \sin(\eta) - P_f^*)) \\ &\quad + (\theta - \bar{\theta})^T M_1^{-1} (M_2 + M_3) (-\theta + P_t) \\ &= - \begin{pmatrix} \omega \\ \mathcal{B}\Gamma (\sin(\eta) - \sin(\bar{\eta})) \end{pmatrix}^T Z \begin{pmatrix} \omega \\ \mathcal{B}\Gamma (\sin(\eta) - \sin(\bar{\eta})) \end{pmatrix} \\ &\quad - (P_t - \theta)^T M_1^{-1} (M_2 + M_3) (P_t - \theta), \end{aligned} \quad (33)$$

where we used (26) in the second equality above and defined

$$Z = \begin{bmatrix} K_p^{-1} - T_p K_p^{-1} X \mathcal{B}\Gamma [\cos(\eta)] \mathcal{B}^T & \frac{1}{2} K_p^{-1} X \\ \frac{1}{2} X K_p^{-1} & X \end{bmatrix}. \quad (34)$$

Since $X \succ 0$, it follows that $\dot{S}_B \leq 0$ if the Schur complement of block X of matrix $\frac{1}{2}(Z + Z^T)$ satisfies

$$\begin{aligned} 0 &< K_p^{-1} - \frac{1}{4} K_p^{-1} X K_p^{-1} - \frac{1}{2} (T_p K_p^{-1} X \mathcal{B}\Gamma [\cos(\eta)] \mathcal{B}^T \\ &\quad + \mathcal{B}\Gamma [\cos(\eta)] \mathcal{B}^T X K_p^{-1} T_p). \end{aligned} \quad (35)$$

The claim then follows from Assumption 5.1. \blacksquare

Now, we can prove the main result of this paper concerning the evolution of the augmented system controlled via the proposed SSOSM control strategy.

Theorem 5.1 (Main result): *Let Assumptions 3.1–5.3 hold. Consider system (4), augmented with the integrators (8) and controlled via (11)–(19). Then, the solutions to the closed-loop system starting in a neighbourhood of the equilibrium $(\bar{\omega} = \mathbf{0}, \bar{\eta}, \bar{P}_t, \bar{P}_g)$ approach the set where $\bar{\omega} = \mathbf{0}$ and $\mathcal{B}\Gamma \sin(\bar{\eta}) = \mathcal{B}P_f^*$, where $\mathcal{B}P_f^*$ is the desired net power exchanged by the control areas.*

Proof: Following Lemma 5.1, we have that the SSOSM control enforces system (4), (8) to evolve $\forall t \geq T_r$ on the sliding manifold characterised by $\sigma = \dot{\sigma} = \mathbf{0}$, resulting in the reduced order system (25). Consider the incremental storage function S_B , given by (28). In view of Lemmas 5.3 and 5.4, we have that S_B has a local minimum at $(\bar{\omega} = \mathbf{0}, \bar{\eta}, \bar{P}_t, \bar{\theta})$ and satisfies along the solutions to (25)

$$\begin{aligned} \dot{S}_B &= - \begin{pmatrix} \omega \\ \mathcal{B}\Gamma (\sin(\eta) - \sin(\bar{\eta})) \end{pmatrix}^T Z \begin{pmatrix} \omega \\ \mathcal{B}\Gamma (\sin(\eta) - \sin(\bar{\eta})) \end{pmatrix} \\ &\quad - (P_t - \theta)^T M_1^{-1} (M_2 + M_3) (P_t - \theta) \\ &\leq 0, \end{aligned} \quad (36)$$

where $Z + Z^T \succ 0$. Consequently, there exists a forward invariant set Υ around $(\bar{\omega} = \mathbf{0}, \bar{\eta}, \bar{P}_t, \bar{\theta})$ and by the Barbashin–Krasovskii–LaSalle invariance principle, the solutions

that start in Υ approach the largest invariant set contained in

$$\Upsilon \cap \{(\omega, \eta, P_t, \theta) : \omega = \mathbf{0}, \mathcal{B}\Gamma \sin(\eta) = \mathcal{B}\Gamma \sin(\bar{\eta}), P_t = \theta\}. \quad (37)$$

From (24), it additionally follows that on the largest invariant set $P_g = P_t$. Bearing in mind that $\mathcal{B}\Gamma \sin(\bar{\eta}) = \mathcal{B}P_f^*$, we can indeed observe that system (4) approaches the set where the frequency deviation is zero, and where the net exchanged power is equal to the desired value, i.e. $\mathcal{B}\Gamma \sin(\eta) = \mathcal{B}P_f^*$. \blacksquare

Remark 5.2 (Acyclic network topologies): In case the topology of the power network does not contain any cycles, we have that the corresponding incidence matrix \mathcal{B} has full column rank (Bapat, 2010, Lemma 2.2) and therefore has a left-inverse satisfying $\mathcal{B}^+ \mathcal{B} = \mathbf{I}$, such that we can conclude from Theorem 1 that the system approaches the set where

$$\begin{aligned} \mathcal{B}\Gamma \sin(\bar{\eta}) &= \mathcal{B}P_f^* \\ \mathcal{B}^+ \mathcal{B}\Gamma \sin(\bar{\eta}) &= \mathcal{B}^+ \mathcal{B}P_f^* \\ \Gamma \sin(\bar{\eta}) &= P_f^*. \end{aligned} \quad (38)$$

Remark 5.3 (Time-varying current demand): We assume that the power demand is constant (see Assumption 5.3), to allow for a steady-state solution (see Assumption 3.1) and to theoretically assess the stability of the power network. Yet, the sliding mode control strategy proposed in Section 4 is still applicable if Assumption 5.3 is removed and the solutions to the power system model will be constrained to the sliding manifold.

Remark 5.4 (Region of attraction): The Barbashin–Krasovskii–LaSalle invariance principle can be applied to all bounded solutions. As follows from Lemma 5.2, we have that on the sliding manifold the considered incremental storage function attains a local minimum at the desired steady state, which allows us to show the existence of a region of attraction once the system evolves on the sliding manifold. Furthermore, the time to converge to the sliding manifold can be made arbitrarily small by properly initialing the system and choosing the gains of the SSOSM control algorithm. To characterise the region of attraction requires a careful analysis of the level sets associated to the incremental storage function S_B , as well as of the trajectories outside of the sliding manifold. Although, a preliminary numerical assessment shows that the region of attraction is large, a thorough analysis of the region of attraction is outside the scope of this paper. An interesting direction is to incorporate techniques developed in Vu and Turitsyn (2016) and Dvijotham, Low, and Chertkov (2015) where energy functions, similar to the one used in this paper, are further characterised.

5.1 Existence and calculation of X

In this subsection, we show that there always exists a diagonal matrix X that satisfies (21) and (22). Furthermore, in order to facilitate the controller tuning, we provide a simple algorithm that permits to compute possible entries of X , that is essentially based on the coming two lemmas. The first lemma determines a diagonal matrix X that satisfies (21).

Lemma 5.4 (X satisfying (21)): If $X = \epsilon_1 K_p T_p^{-1}$, with

$$\epsilon_1 < \min_{i \in \mathcal{V}} \left(\sqrt{\frac{T_{pi}}{2K_{pi} \sum_{k \in \mathcal{N}_i} \Gamma_k}} \right), \quad (39)$$

then (21) is satisfied.

Proof: Note that, after the substitution $X = \epsilon_1 K_p T_p^{-1}$, (21) becomes

$$0 < T_p K_p^{-1} - \epsilon_1^2 \mathcal{B} \Gamma [\cos(\bar{\eta})] \mathcal{B}^T, \quad (40)$$

which holds if the largest eigenvalue λ_{\max} satisfies

$$\lambda_{\max}(\epsilon_1^2 T_p^{-1} K_p \mathcal{B} \Gamma [\cos(\bar{\eta})] \mathcal{B}^T) < 1. \quad (41)$$

By the Gershgorin circle theorem, every eigenvalue of $\epsilon_1^2 T_p^{-1} K_p \mathcal{B} \Gamma [\cos(\bar{\eta})] \mathcal{B}^T$ lies within at least one of the Gershgorin disk $D_i(c_i, r_i)$ centred at c_i , and with radius r_i , where

$$c_i = r_i = \epsilon_1^2 T_{pi}^{-1} K_{pi} \sum_{k \in \mathcal{N}_i} |\Gamma_k \cos(\bar{\eta}_k)|, \quad (42)$$

where \mathcal{N}_i is the set of lines connecting control area i . We therefore have that

$$\lambda_{\max}(\epsilon_1^2 T_p^{-1} K_p \mathcal{B} \Gamma [\cos(\bar{\eta})] \mathcal{B}^T) < 1. \quad (43)$$

if

$$\epsilon_1 < \min_{i \in \mathcal{V}} \left(\sqrt{\frac{T_{pi}}{2K_{pi} \sum_{k \in \mathcal{N}_i} \Gamma_k}} \right). \quad (44)$$

■

Similarly, the second lemma determines a diagonal matrix X that satisfies (22).

Lemma 5.5 (X satisfying (22)): If $X = \epsilon_2 K_p T_p^{-1}$, with

$$\epsilon_2 < \min_{i \in \mathcal{V}} \left(\frac{T_{pi}}{\frac{1}{2} + 2K_{pi} T_{pi} \sum_{k \in \mathcal{N}_i} \Gamma_k} \right). \quad (45)$$

then (22) is satisfied.

Proof: Note that, after the substitution $X = \epsilon_2 K_p T_p^{-1}$, (22) becomes

$$0 < K_p^{-1} \left(I - \frac{1}{4} \epsilon_2 T_p^{-1} \right) - \epsilon_2 \mathcal{B} \Gamma [\cos(\eta)] \mathcal{B}^T, \quad (46)$$

which holds, in analogy to Lemma 5.4, if

$$\lambda_{\max} \left(\epsilon_2 K_p \left(I - \frac{1}{4} \epsilon_2 T_p^{-1} \right)^{-1} \mathcal{B} \Gamma [\cos(\eta)] \mathcal{B}^T \right) < 1. \quad (47)$$

Following the same argument as in Lemma 5.4, applying the Gershgorin circle theorem, we have that (22) is satisfied when

$$\epsilon_2 < \min_{i \in \mathcal{V}} \left(\frac{T_{pi}}{\frac{1}{2} + 2K_{pi} T_{pi} \sum_{k \in \mathcal{N}_i} \Gamma_k} \right). \quad (48)$$

■

From Lemmas 5.4 and 5.5, the following corollary is immediate and indeed shows that there always exists a diagonal matrix X that satisfies (21) and (22):

Corollary 5.1 (X satisfying (21) and (22)): Let

$$X = \epsilon K_p T_p^{-1}, \quad (49)$$

with $\epsilon = \min\{\epsilon_1, \epsilon_2\}$, then (21) and (22) are satisfied.

Remark 5.5 (A simple algorithm to determine X): The results of this subsection can be straightforwardly adapted to design an algorithm to determine a suitable local value X_{ii} at every control area $i \in \mathcal{V}$. First, every area determines an upper bound for $\bar{\epsilon}_i$ using (39) and (45)

$$\bar{\epsilon}_i = \min \left\{ \sqrt{\frac{T_{pi}}{2K_{pi} \sum_{k \in \mathcal{N}_i} \Gamma_k}}, \frac{T_{pi}}{\frac{1}{2} + 2K_{pi} T_{pi} \sum_{k \in \mathcal{N}_i} \Gamma_k} \right\} \quad (50)$$

Notice that determining $\bar{\epsilon}_i$ only requires the use of locally available information. Second, the obtained upper bounds are broadcasted to the other areas within the network such that all areas $i \in \mathcal{V}$ can obtain a value of $\epsilon = \min_{i \in \mathcal{V}} \{\bar{\epsilon}_i\}$. Third, if every area selects $X_{ii} = \epsilon K_{pi} T_{pi}^{-1}$, it is ensured that X satisfies (21) and (22).

6. Simulation results

In this section, the proposed control solution is assessed in simulation⁶ on a power network partitioned into four control areas.

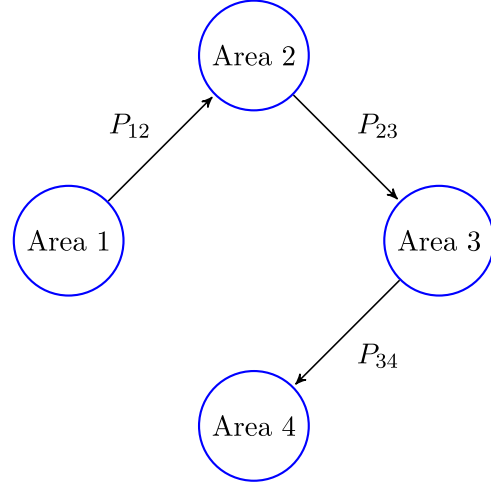


Figure 2. Scheme of the considered power network partitioned into four control areas, where $p_{ij} = \frac{V_i^* V_j}{X_{ij}} \sin(\delta_i - \delta_j)$. The arrows indicate the positive direction of the power flows through the power network.

Table 2. An overview of the numerical values used in the simulations, where a base power of 1000 MW is assumed.

		Area 1	Area 2	Area 3	Area 4
T_{pi}	(s)	21.0	25.0	23.0	22.0
T_{ij}	(s)	0.30	0.33	0.35	0.28
T_{gi}	(s)	0.080	0.072	0.070	0.081
K_{pi}	(ϵ^{-1} p.u. ⁻¹)	120.0	112.5	115.0	118.5
R_i	(ϵ^{-1} p.u. ⁻¹)	2.5	2.7	2.6	2.8
$T_{\theta i}$	(s)	0.1	0.1	0.1	0.1
$P_{di}(0)$	(p.u.)	0.010	0.014	0.012	0.013
$P_{di}(1)$	(p.u.)	0.020	0.028	0.024	0.026

The topology of the power network is represented in Figure 2, and it is described by the incidence matrix

$$B = \begin{bmatrix} 1 & 0 & 0 \\ -1 & 1 & 0 \\ 0 & -1 & 1 \\ 0 & 0 & -1 \end{bmatrix}.$$

According to the choice of B , the arrow on each edge of the graph in Figure 2 indicates the positive direction of the power flow. The relevant network parameters of each area are provided in Table 2, where a base power of 1000 MW is assumed. The line parameters are $\gamma_1 = \gamma_2 = \gamma_3 = 0.1$ p.u., while the scheduled power flows are $P_{f1}^* = 0.015$ p.u., $P_{f2}^* = 0.0125$ p.u. and $P_{f3}^* = 0.01$ p.u. Let $I_4 \in \mathbb{R}^{4 \times 4}$ be the identity

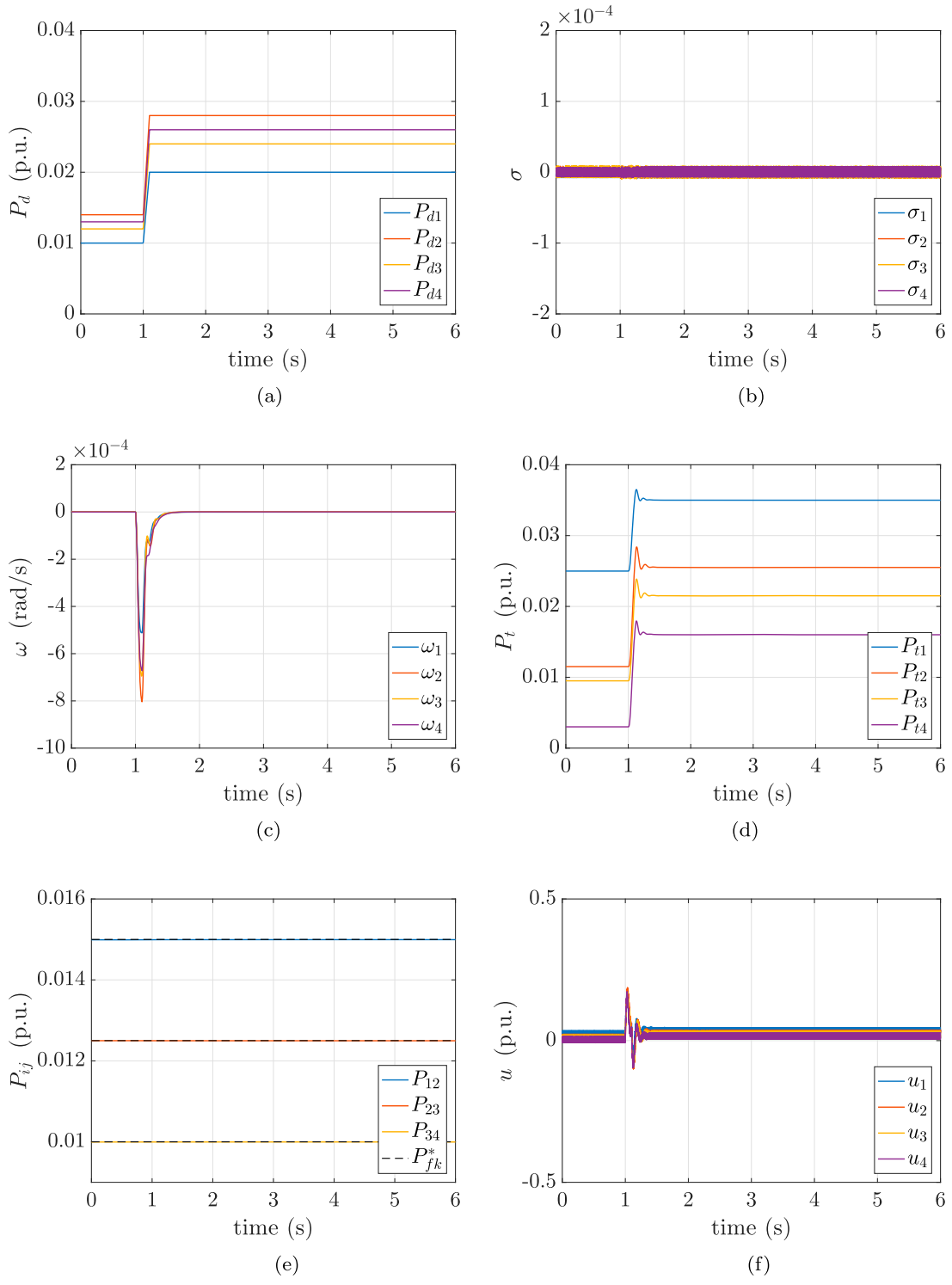


Figure 3. (Scenario 1). Power demands, sliding variables, frequency deviations, turbine output powers, power flows on every line and control inputs. The proposed controllers are used with X satisfying (49). (a) Power demands, (b) sliding variables, (c) frequency deviations, (d) turbine output powers, (e) power flows and (f) control inputs.

matrix. The matrices in (11) are chosen as $M_1 = 2 \mathbf{I}_4$, $M_2 = 0.1 \mathbf{I}_4$, $M_3 = 0.01 \mathbf{I}_4$, $M_4 = -(M_2 + M_3)$, and $M_5 = M_1 X = \epsilon M_1 K_p T_p^{-1}$, with $\epsilon = 0.0217$. The control amplitude W_{\max_i} and the parameter α_i^* , in (17) are selected equal to 500 and 1, respectively, for all $i \in \{1, 2, 3, 4\}$. Initially, the system is at the steady state with power demand $P_{di}(0)$ in area $i \in \{1, 2, 3, 4\}$ (see Table 2). In order to investigate the performance of the proposed control approach within a power network, five different

scenarios are implemented. In the last one, we show that when Assumption 5.1 is not satisfied, the controlled power network can become unstable.

6.1 Scenario 1: step variation of the power demand

At the time instant $t=1$ s, the power demand in each area becomes $P_{di}(1)$ (see Table 2 and Figure 3(a)). From Figure 3(b),

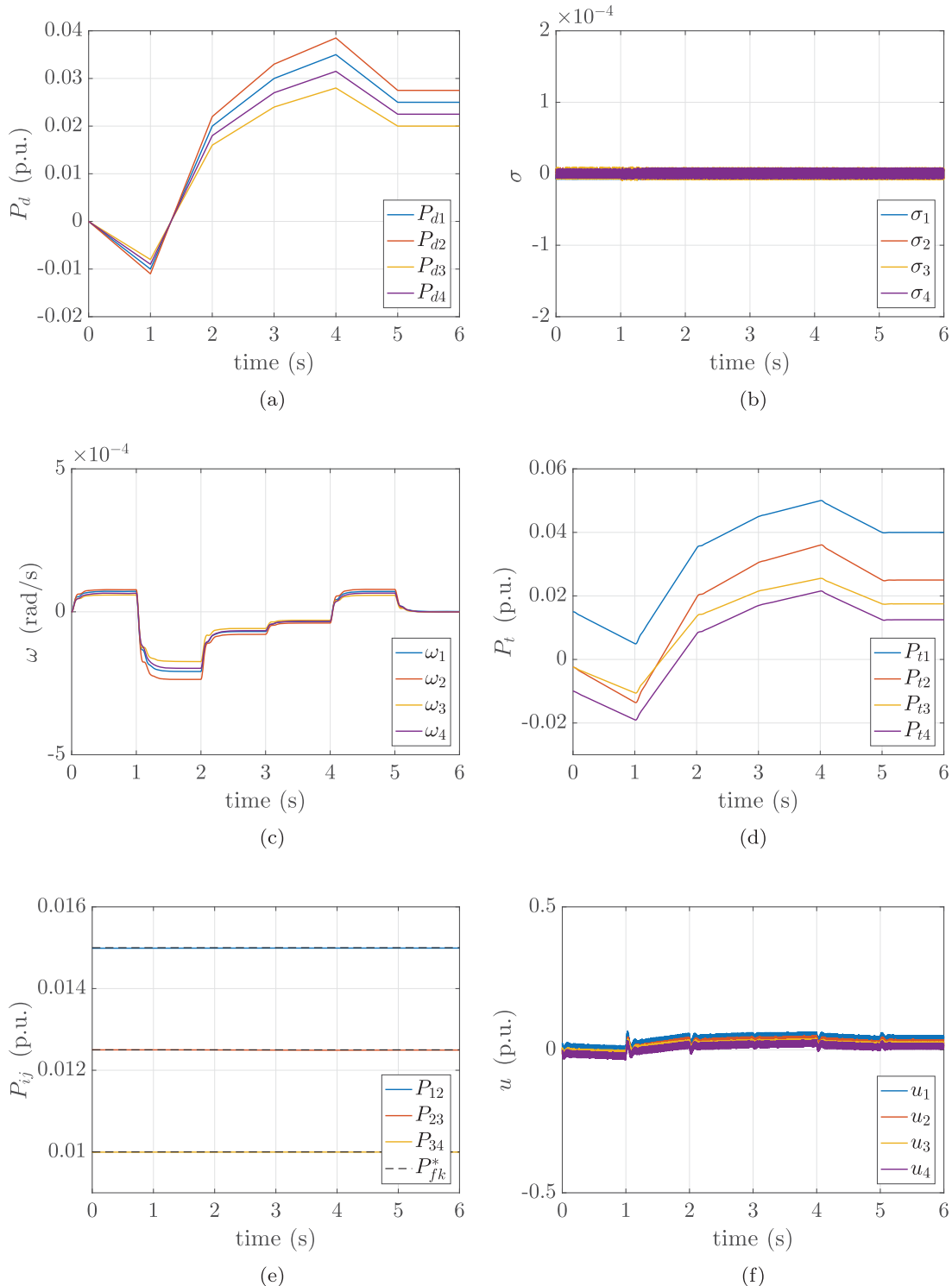


Figure 4. (Scenario 2). Power demands, sliding variables, frequency deviations, turbine output powers, power flows on every line and control inputs. The proposed controllers are used with X satisfying (49). (a) Power demands, (b) sliding variables, (c) frequency deviations, (d) turbine output powers, (e) power flows and (f) control inputs.

one can observe that the sliding variables are kept to the manifold $\sigma = \mathbf{0}$. Furthermore, the frequency deviations converge asymptotically to zero after a transient during which the frequency drops because of the increasing load (see Figure 3(c)). From Figure 3(d) one can note that the proposed controllers increase the power generation in order to reach again a zero steady-state frequency deviation, while maintaining, at the steady state, the scheduled power flows P_{fk}^* on each

line (see Figure 3(e)). In Figure 3(f), the control inputs are shown.

6.2 Scenario 2: time-varying power demand

In this scenario, the power demand continuously changes during the simulation time interval as shown in Figure 4(a). From Figure 4(b), one can observe that the sliding variables are

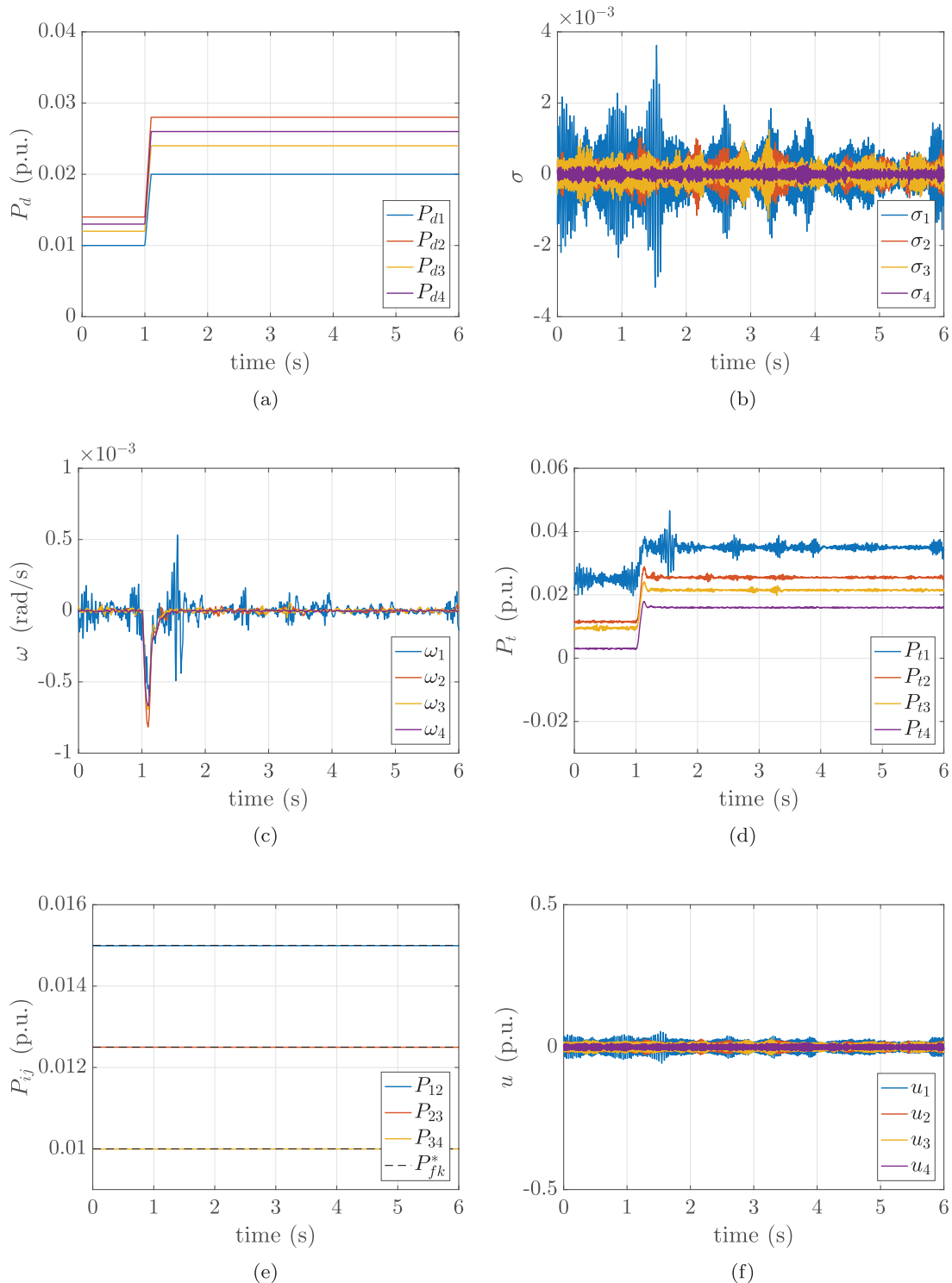


Figure 5. (Scenario 3). Power demands, sliding variables, frequency deviations, turbine output powers, power flows on every line and control inputs, considering noises in the frequency measurements. The proposed controllers are used with X satisfying (49). (a) Power demands, (b) sliding variables, (c) frequency deviations, (d) turbine output powers, (e) power flows and (f) control inputs.

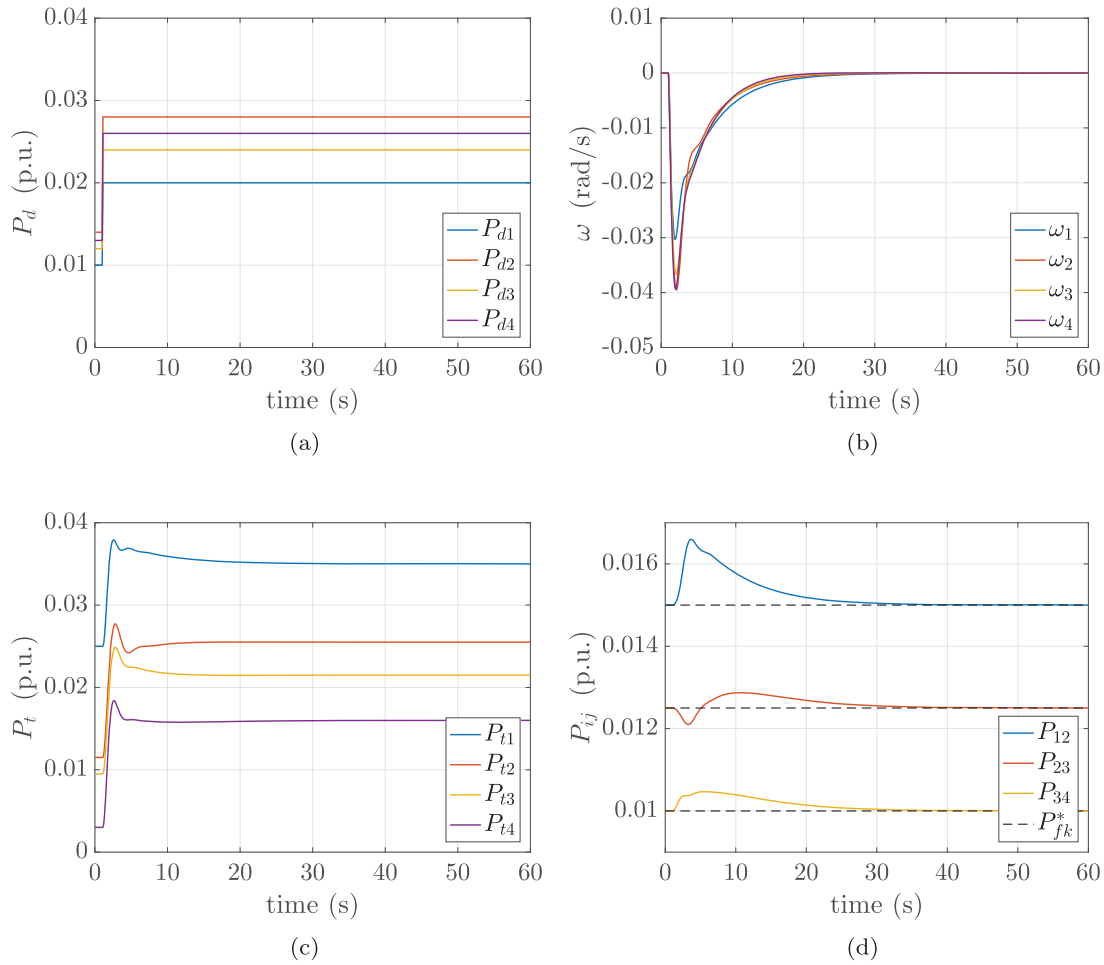


Figure 6. (Scenario 4). Power demands, frequency deviations, turbine output powers and power flows on every line. The control law (51) proposed in Kundur et al. (1994) is used. (a) Power demands, (b) frequency deviations, (c) turbine output powers and (d) power flows.

kept to the manifold $\sigma = \mathbf{0}$. Since the power demand is an unknown unmatched external disturbance, the frequency deviations evolve until the power demand becomes constant (see Figure 4(c)). From Figure 4(d), one can note that the proposed controllers continuously adjust the power generation in order to reach again a zero steady-state frequency deviation when the power demand becomes constant. The scheduled power flows P_{fk}^* on each line are maintained even during the transient (see Figure 4(e)). In Figure 4(f), the control inputs are shown.

6.3 Scenario 3: measurement noises

Here, we repeat Scenario 1 adding noises in the frequency measurements. At the time instant $t = 1$ s, the power demand in each area becomes $P_{di}(1)$ (see Table 2 and Figure 5(a)). From Figure 5(b), one can observe that the sliding variables converge to a vicinity of the origin. Also the frequency deviations converge asymptotically to a vicinity of the origin after a transient during which the frequency drops because of the increasing load (see Figure 5(c)). From Figure 5(d) one can note that the proposed controllers increase the power generation, while maintaining the scheduled power flows P_{fk}^* on each line (see Figure 5(e)). In Figure 5(f) the control inputs are shown.

6.4 Scenario 4: comparison with Kundur et al. (1994)

In this subsection, the proposed controller is compared with the conventional automatic generation control law proposed in Kundur et al. (1994), which is given by

$$u_i(t) = -K_{fi} \int_0^t ACE_i(\tau) d\tau, \quad (51)$$

where ACE_i is known as *area control error* and is given by

$$ACE_i(t) = \left(\mathcal{B}\Gamma \sin(\eta) - \mathcal{B}P_f^* \right)_i + b_i \omega_i, \quad (52)$$

$b_i = 1/R_i + 1/K_{pi}$ being a suitable *bias factor* for all areas $i \in \mathcal{V}$ (see Kundur et al., 1994 for more details). We select $K_{fi} = -0.2$ and repeat Scenario 1, i.e. at the time instant $t = 1$ s, the power demand in each area becomes $P_{di}(1)$ (see Table 2 and Figure 6(a)). The resulting frequency deviations, turbine output powers and line power flows are provided in Figure 6(b–d), respectively. In comparison with the proposed control scheme in this work (see Figure 3(c–e)), one can notice that the overall response when controller (51) is used, is much slower (note that in the considered scenario the simulation horizon is ten times longer than all the previous scenarios), with larger frequency drops and power flow deviations from the corresponding scheduled values.

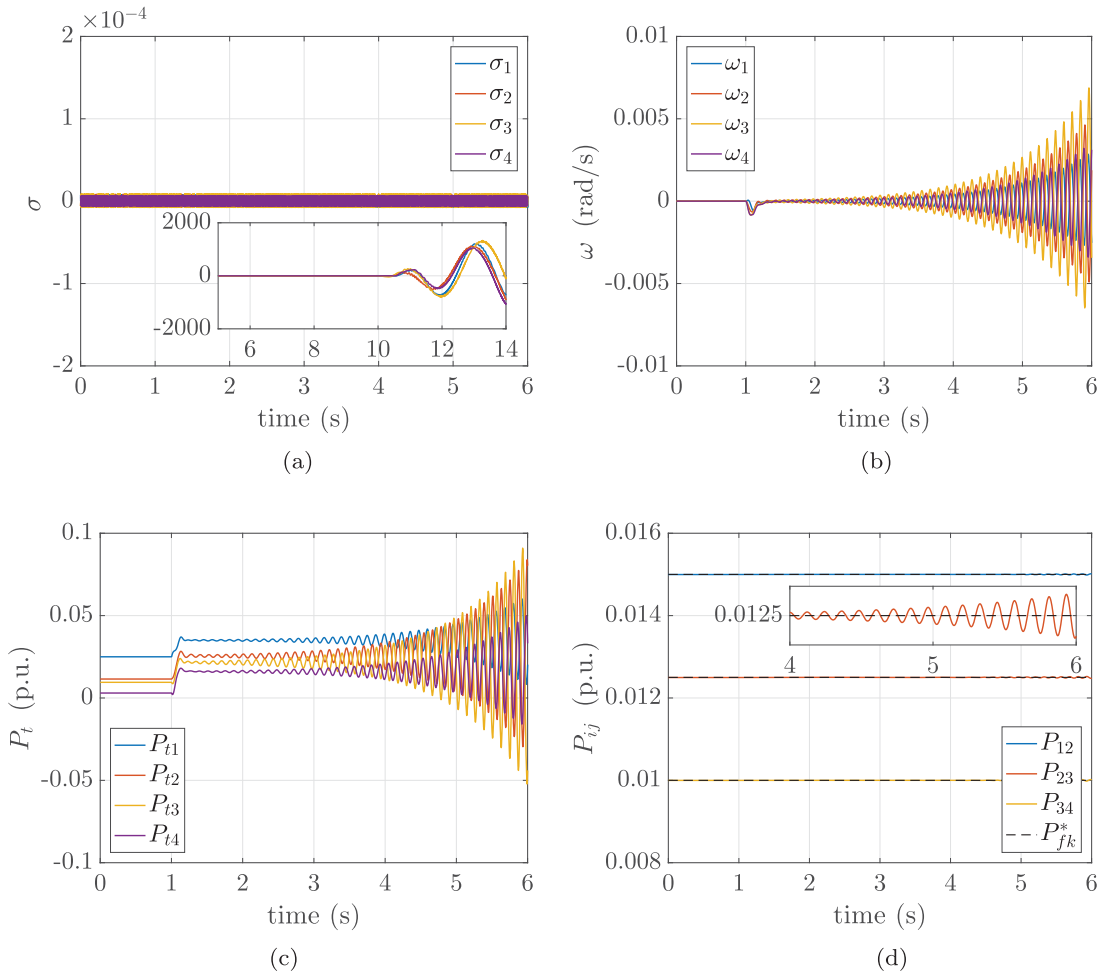


Figure 7. (Scenario 5). Sliding variables, frequency deviations, turbine output powers and power flows on every line. The proposed controllers are used with X not satisfying Assumption 5.1. (a) Sliding variables, (b) frequency deviations, (c) turbine output powers and (d) power flows.

6.5 Scenario 5: condition (49) is not satisfied

To show the importance of the chosen value for ϵ , we replicate Scenario 1 with $\epsilon = 19.5$. One can confirm that this value of ϵ does not satisfy (49). In Figure 7, it is shown that the system, due to the increased value of ϵ , becomes unstable. Particularly, one can notice that after the system being initially at steady state, the change in power demand causes oscillation of the various states with growing amplitude. Although the system is kept on the sliding manifold for a limited amount of time, the growing amplitude of the various oscillations eventually causes that the sliding condition cannot longer be maintained (see Figure 7 (a)).

7. Conclusions

A decentralised SSOSM control scheme is proposed for LFC. We considered a power network partitioned into control areas, where each area is modelled by an equivalent generator including second-order turbine-governor dynamics, and where the areas are nonlinearly coupled through the power flows. Relying on stability considerations made on the basis of an incremental energy (storage) function, a suitable nonlinear sliding function is designed. Local asymptotic convergence is

proven to the state where the frequency deviation is zero and where the (net) power flows are identical to their desired values.

Notes

1. For the sake of simplicity, the order r of the sliding manifold is omitted in the remainder of this paper.
2. In case the ‘internal’ governor state P_{gi} or the frequency deviation ω cannot be measured directly, one can rely, e.g. on the sliding mode observers proposed in Rinaldi, Cucuzzella, and Ferrara (2017, 2018) to estimate their values in finite time.
3. The relative degree is the minimum order r of the time derivative $\sigma_i^{(r)}$, $i \in \{1, \dots, n\}$, of the sliding variable associated to the i th node in which the control u_i , $i \in \{1, \dots, n\}$, explicitly appears.
4. The peak detector proposed in Bartolini et al. (1998b) requires only the measurement of the sliding function σ , which converges to a ρ^2 -vicinity of the origin, where $\rho > 0$ is an arbitrarily small positive constant.
5. Let $[\cos(\eta)]$ denote the $m \times m$ diagonal matrix $\text{diag}\{\cos(\eta_1), \dots, \cos(\eta_m)\}$.
6. The power network is modelled in MATLAB-Simulink R2018a by using the forward Euler method with sampling time interval $\tau_s = 1 \times 10^{-3}$ s. Then, according to Shtessel et al. (2014), the corresponding discrete-sampling version provides an accuracy level of $\sigma = O(\tau_s^2)$, $\dot{\sigma} = O(\tau_s)$.

Disclosure statement

No potential conflict of interest was reported by the authors.

Funding

This work is supported by the EU Project 'MatchIT' (project number: 82203).

ORCID

Sebastian Trip  <http://orcid.org/0000-0002-6766-6857>

References

- Apostolopoulou, D., Domínguez-García, A. D., & Sauer, P. W. (2016, July). An assessment of the impact of uncertainty on automatic generation control systems. *IEEE Transactions on Power Systems*, 31(4), 2657–2665.
- Bapat, R. B. (2010). *Graphs and matrices*. Springer.
- Bartolini, G., Ferrara, A., & Usai, E. (1998a, February). Chattering avoidance by second-order sliding mode control. *IEEE Transactions on Automatic Control*, 43(2), 241–246.
- Bartolini, G., Ferrara, A., & Usai, E. (1998b, September). On boundary layer dimension reduction in sliding mode control of SISO uncertain nonlinear systems. *Proceedings of the IEEE international conference on control applications* (pp. 242–247). Trieste, Italy.
- Bregman, L. (1967). The relaxation method of finding the common point of convex sets and its application to the solution of problems in convex programming. *USSR Computational Mathematics and Mathematical Physics*, 7(3), 200–217.
- Chang, C., & Fu, W. (1997, August). Area load frequency control using fuzzy gain scheduling of PI controllers. *Electric Power Systems Research*, 42(2), 145–152.
- Dong, L. (2016, July). Decentralized load frequency control for an interconnected power system with nonlinearities. *Proceedings of the IEEE American control conference* (pp. 5915–5920). Boston, MA.
- Dvijotham, K., Low, S., & Chertkov, M. (2015). Convexity of energy-like functions: Theoretical results and applications to power system operations. *arXiv preprint arXiv:1501.04052v3*.
- Edwards, C., & Spurgeon, S. K. (1998). *Sliding mode control: Theory and applications*. London: Taylor and Francis.
- Ersdal, A. M., Imsland, L., & Uhlen, K. (2016, January). Model predictive load-frequency control. *IEEE Transactions on Power Systems*, 31(1), 777–785.
- Furtat, I. B., & Fradkov, A. L. (2015, December). Robust control of multi-machine power systems with compensation of disturbances. *International Journal of Electrical Power & Energy Systems*, 73, 584–590.
- Ha, Q. P. (1998, April). A fuzzy sliding mode controller for power system load-frequency control. *Knowledge-based intelligent electronic systems* (pp. 149–154). Adelaide, SA.
- Ibraheem, N., Kumar, P., & Kothari, D. P. (2005, February). Recent philosophies of automatic generation control strategies in power systems. *IEEE transactions on Power Systems*, 20(1), 346–357.
- Incremona, G. P., Cucuzzella, M., & Ferrara, A. (2016, January). Adaptive suboptimal second-order sliding mode control for microgrids. *International Journal of Control*, 89(9), 1849–1867.
- Kundur, P., Balu, N. J., & Lauby, M. G. (1994). *Power system stability and control*. New York, NY: McGraw-hill.
- Levant, A. (1993). Sliding order and sliding accuracy in sliding mode control. *International Journal of Control*, 58(6), 1247–1263.
- Levant, A. (2003, January). Higher-order sliding modes, differentiation and output-feedback control. *International Journal of Control*, 76(9–10), 924–941.
- Mi, Y., Fu, Y., Li, D., Wang, C., Loh, P. C., & Wang, P. (2016, January). The sliding mode load frequency control for hybrid power system based on disturbance observer. *International Journal of Electrical Power and Energy Systems*, 74, 446–452.
- Mi, Y., Fu, Y., Wang, C., & Wang, P. (2013, November). Decentralized sliding mode load frequency control for multi-area power systems. *IEEE Transactions on Power Systems*, 28(4), 4301–4309.
- Pandey, S. K., Mohanty, S. R., & Kishor, N. (2013, September). A literature survey on load-frequency control for conventional and distribution generation power systems. *Renewable and Sustainable Energy Reviews*, 25, 318–334.
- Pogromsky, A. Y., Fradkov, A. L., & Hill, D. J. (1996, December). Passivity based damping of power system oscillations. *Proceedings of 35th IEEE conference on decision and control* (pp. 3876–3881). Kobe.
- Prasad, S., Purwar, S., & Kishor, N. (2015, September). On design of a nonlinear sliding mode load frequency control of interconnected power system with communication time delay. *Proceedings of the IEEE conference on control applications* (pp. 1546–1551). Sydney.
- Rinaldi, G., Cucuzzella, M., & Ferrara, A. (2017, October). Third order sliding mode observer-based approach for distributed optimal load frequency control. *IEEE Control Systems Letters*, 1(2), 215–220.
- Rinaldi, G., Cucuzzella, M., & Ferrara, A. (2018). Sliding mode observers for a network of thermal and hydroelectric power plants. *Automatica*, 98, 51–57.
- Shtessel, Y., Edwards, C., Fridman, L., & Levant, A. (2014). Conventional sliding mode observers. In *Sliding mode control and observation* (pp. 105–141). Springer.
- Trip, S., Bürger, M., & De Persis, C. (2016). An internal model approach to (optimal) frequency regulation in power grids with time-varying voltages. *Automatica*, 64, 240–253.
- Trip, S., Cucuzzella, M., Ferrara, A., & De Persis, C. (2017, July). An energy function based design of second order sliding modes for automatic generation control. *IFAC-PapersOnLine*, 50(1), 11613–11618. (20th IFAC World Congress)
- Trip, S., Cucuzzella, M., Persis, C. D., van der Schaft, A., & Ferrara, A. (2018). Passivity-based design of sliding modes for optimal load frequency control. *IEEE Transactions on Control Systems Technology*.
- Trip, S., & De Persis, C. (2018, September). Distributed optimal load frequency control with non-passive dynamics. *IEEE Transactions on Control of Network Systems*, 5(3), 1232–1244.
- Utkin, V. (2016, March). Discussion aspects of high-order sliding mode control. *IEEE Transactions on Automatic Control*, 61(3), 829–833.
- Utkin, V. I. (1992). *Sliding modes in control and optimization*. Springer-Verlag.
- Ventura, U. P., & Fridman, L. (2016, June). Chattering measurement in SMC and HOSMC. *2016 14th international workshop on variable structure systems (VSS)* (pp. 108–113). Nanjing.
- Vrdoljak, K., Perić, N., & Petrović, I. (2010, May). Sliding mode based load-frequency control in power systems. *Electrical Power Systems Research*, 80(5), 514–527.
- Vu, T. L., & Turitsyn, K. (2016, March). Lyapunov functions family approach to transient stability assessment. *IEEE Transactions on Power Systems*, 31(2), 1269–1277.
- Zribi, M., Al-Rashed, M., & Alrifai, M. (2005, October). Adaptive decentralized load frequency control of multi-area power systems. *International Journal of Electrical Power and Energy Systems*, 27(8), 575–583.